2014

# A Systematic Study on the Mesomorphic Behavior of Asymmetrical 1-Alkyl-3-dodecylimidazolium Bromides

Mei Yang
*Ruhr-Universitat Bochum*

Bert Mallick
*Ruhr-Universitat Bochum*

Anja V. Mudring
*Iowa State University*, mudring@iastate.edu

CRYSTAL GROWTH & DESIGN

Article

pubs.acs.org/crystal

# A Systematic Study on the Mesomorphic Behavior of Asymmetrical 1-Alkyl-3-dodecylimidazolium Bromides

Mei Yang,[†] Bert Mallick,[†] and Anja-Verena Mudring*[,†,‡]

[†]Anorganische Chemie III – Materials Engineering and Characterization, Fakultät für Chemie and Biochemie, Ruhr-Universität Bochum, 44780 Bochum, Germany

[‡]Department of Materials Science and Engineering, Iowa State University and Ames Laboratory, Ames, Iowa 50011, United States

Supporting Information

**ABSTRACT:** To determine the essential parameters for mesophase formation in imidazolium-based ionic liquids (ILs), a library of 1-alkyl-3-dodecylimidazolium bromides was synthesized, abbreviated as CnC12, where $0 \leq n \leq 13$, as the general notion is that a dodecyl side chain would guarantee the formation of an ionic liquid crystal (ILC). All salts were fully characterized by NMR spectroscopy and mass spectrometry. Their thermal properties were recorded, and mesophase formation was assessed. An odd–even effect is observed for $5 \leq n \leq 10$ in the temperatures of melting transitions. While the majority of this series, as expected, formed mesophases, surprisingly compounds C2C12 and C6C12 could not be classified as ILCs, the latter being a room temperature IL, while C2C12 is a crystalline solid with melting point at 37 °C. The single crystal structure of compound 1-ethyl-3-dodecylimidazolium bromide (C2C12) was successfully obtained. Remarkably, the arrangement of imidazolium cores in the structure is very complicated due to multiple nonclassical hydrogen bonds between bromide anions and imidazolium head groups. In this arrangement, neighboring imidazolium rings are forced by hydrogen bonds to form a "face-to-face" conformation. This seems to be responsible for the elimination of a mesophase. To conclude, the general view of a dodecyl chain being a functional group to generate a mesophase is not entirely valid.

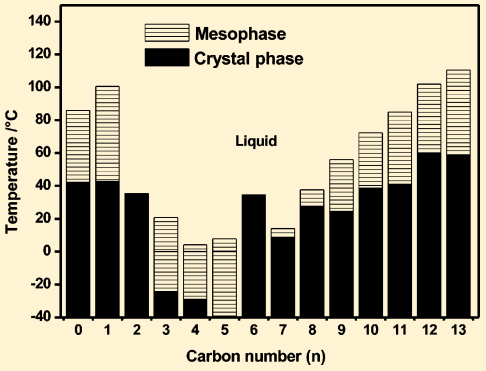


## 1. INTRODUCTION

Ionic liquid crystals (ILCs) are a class of ionic liquid (IL) materials possessing the ability to form a liquid crystalline state. The liquid crystalline state is an intermediate state between perfect ordered crystalline solid state and that of the total disordered liquid state. The molecules in this state are ordered along at least one spatial coordinate.[1] ILCs are ionic compounds and are also amphiphiles in general. Their physiochemical properties such as melting points, viscosity, conductivity, and lipophilicity can be tuned by varying cation and anion combinations like in ILs.[2] The combination of the partially ordered properties and IL features of these amphiphilic compounds has rendered them one of the most attractive materials. The physicochemical properties of ILCs have been extensively studied based on their structural changes.[3−7] The importance of ILCs has been realized in diverse applications, such as ion-conductive materials,[8] organized reaction media, or self-assembled nanostructured materials.[1,9,10] Thanks to the formation of ordered domains, in which reactions could occur, if used as reaction media ILCs may supply an additional reaction control.[11−14] In addition, ILCs may also exhibit catalytic activities and/or play an important role in selectivity.[15] For example, ILCs and long chain alkyl ILs have been used in an "ILC-SILP" (SILP: supported ionic liquid phases) concept for a "medium induced selectivity" during Ni-NHC-catalyzed olefin dimerization.[16,17] Although they are also highly attractive functional materials and have attracted significantly increasing interest in recent years, ILCs have not received the same in-depth attention.

Nowadays, imidazolium-based cations are by far the most popular examples for both ILs and ILCs.[18−21] The correlation between the properties and structural changes of imidazolium-based ILs has been systematically investigated, regarding a wide variety of changing cationic and anionic structures.[3,4,6] The fundamental understanding of the effect of alkyl groups on physiochemical properties, including thermal behavior, viscosity, density, and microscopic ion dynamics has been reported. According to the findings of us and others,[22] a dodecyl unit could be considered as a functional group responsible for liquid crystalline behavior; that is, for 1-alkyl-3-methylimidazolium, mesomorphism can be observed when the alkyl chain contains 12 or more carbon atoms.[6] However, with regard to these long chain-bearing ILs, only 1-alkyl-3-methylimidazolium and symmetrical 1,3-dialkylimidazoliums (where alkyl ≥ dodecyl) have been investigated for their ILC behavior. Only little is understood with respect to the fundamental aspects of LC formation from asymmetric long chain 1,3-dialkylimidazolium compounds. Correlation of varying alkyl chain length with the

Received: September 19, 2013
Revised: February 11, 2014
Published: February 12, 2014

   dx.doi.org/10.1021/cg401396n | Cryst. Growth Des. 2014, 14, 1561−1571

changes in physicochemical properties of ILs bearing one dodecyl unit still needs to be explored to facilitate the molecular design of ILCs. Furthermore, previous investigations of imidazolium-based ILs and ILCs have mostly focused on even numbered chain lengths; ILs or ILCs with odd number alkyl chains are very seldom reported.

For this reason, a series of 1-alkyl-3-dodecylimidazolium bromides ([CnC12IM]Br, $n$ = 0 − 13) was investigated. The influence of these systematic structural variations on the physicochemical properties was studied, focusing on their thermal behavior and liquid crystalline properties. The thermal and structural properties were investigated via differential scanning calorimetry (DSC), polarizing optical microscopy (POM), and temperature dependent X-ray diffraction (SAXS).

For convenience, we use the same designations for the compounds as is used in our previous report.[22] The compounds are named by the number of carbon atoms in the two alkyl chains at the first and third positions of the imidazolium ring. For example, [C5IMC12]Br, 1-pentyl-3-dodecylimidazolium bromide, as C5C12 and [C6IMC12]Br, 1-hexyl-3-dodecylimidazolium bromide, as C6C12.

## 2. EXPERIMENTAL SECTION

**2.1. Sample Preparation.** The synthesis and sample handling of anhydrous salts were carried out using standard Schlenk and argon-glovebox techniques. All the bromide compounds were hygroscopic. The samples were dried under $10^{-6}$ mbar at 60 °C for 3 days. All the sample preparations for further analytics were carried out in an argon-glovebox.

**2.2. Synthesis.** Acetonitrile (99.5%), ethyl acetate (95%), methanol (99%), dichloromethane (99.9%), and tetrahydrofuran (extra dry, >99%) were used as received from J.T. Backer (Deventer, Holland). Hydrobromic acid (47%) was obtained from Merck (Darmstadt, Germany). 1-Propylimidazole (98%), 1-hexylimidazole (98%), and 1-octylimidazole (98%) were purchased from IoLiTec (Heilbronn, Germany). 1-Ethylimidazole (95%), 1-butylimidazole (98%), imidazole (99.5%), sodium hydride (95%), and all 1-bromoalkanes were purchased from Sigma-Aldrich (Steinheim, Germany). All chemicals were used as received without further purification.

**Scheme 1. 1-Alkyl-3-dodecylimidazolium Cations under Investigation**[a]

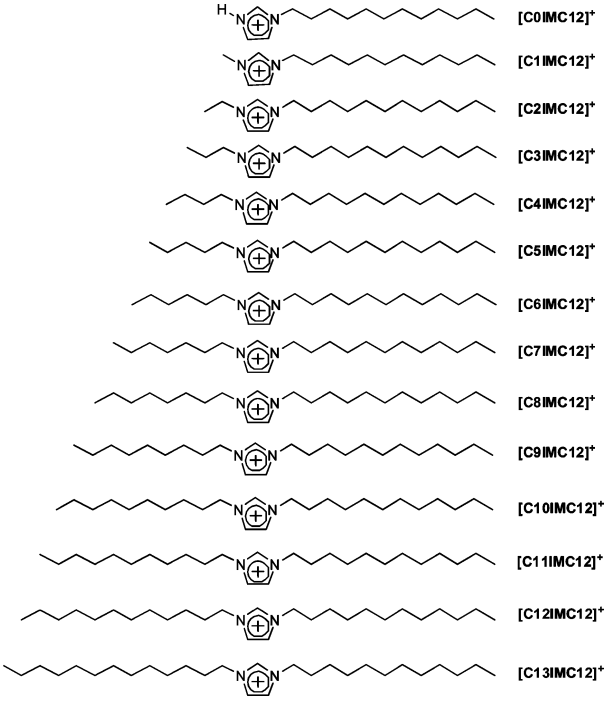


[a]Bromide was used as the counter ion.

*1-Dodecylimidazole* was synthesized using a reported procedure.[20] After the purification procedure, the product was obtained as a yellow-brownish oil. Experimental details are provided in Supporting Information. Yield = 71%. $^1$H NMR (298 K, 200 MHz, DMSO-$d_6$): $\delta$ [ppm] = 0.86 (3H, t), 1.04−1.46 (14H, m), 1.64−1.83 (2H, m), 3.71−4.09 (2H, m), 6.92 (2H, dd), 7.43 (1H, s).

*[C0C12]Br* was prepared by dropwise addition of a slight excess of concentrated hydrobromic acid (4 mL) to 1-dodecylimidazole at 0 °C (1.0 g, 4.2 mmol) in diethyl ether. The bromide salt precipitated as a white solid after cooling at −30 °C overnight. Unlike [C0C13]Br,[22] [C0C12]Br was highly hygroscopic. The product was filtered under inert environment, washed repeatedly with ethyl acetatem and dried in a vacuum for at least 3 days at 60 °C. Yield = 48%. $^1$ H NMR (200 MHz, DMSO-$d_6$): $\delta$ [ppm] = 0.83 (3H, t), 1.22 (22H, m), 1.78 (2H, t), 4.16 (2H, t), 7.68 (1H, s), 7.78 (1H, s), 9.15 (1H, s). ESI-MS (positive, ([%])) $m/z$ = 265.1 [M − Br]$^+$ (100).

*C5C12, C7C12, C9C12, C10C12, C11C12, C12C12,* and *C13C12* were synthesized with the general method for 1,3-dialkylimidazolium bromides via direct alkylation of the respective 1-dodecylimidazole with alkyl bromide in a 1:1.1 molar ratio in acetonitrile.[23]

Syntheses of *C1C12, C2C12, C3C12, C4C12, C6C12,* and *C8C12* followed the same procedure except 1-methylimidazole, 1-ethylimidazole, 1-propylimidazole, 1-butylimidazole, 1-hexylimidazole, and 1-octylimidazole were alkylated using 1-bromododecane.

Compounds C0C12, C1C12, and C2C12 were obtained as crystalline solids; compounds C3C12, C4C12, and C5C12 are viscous room temperature ionic liquids (RTILs); C6C12 is obtained as a crystalline solid, while C7C12, C8C12, C9C12, and C10C12 are viscous liquids or wax-like solids. The analytical data are reported below.

*[C1C12]Br* was synthesized from 1-methylimidazole (2.5 g, 30.0 mmol) and 1-bromododecane (8.3 g, 33.0 mmol). Yield = 91%. $^1$H NMR (298 K, 200 MHz, DMSO-$d_6$) $\delta$ [ppm] = 0.82 (3H, t), 1.20 (17H, m), 1.74(2H, t), 3.81 (s, 3H), 4.17 (2H, t), 7.61 (2H, s), 9.27 (1H, s). ESI-MS (positive, ([%])) $m/z$ = 251.1 [M − Br]$^+$ (100).

*[C2C12]Br* was synthesized from 1-ethylimidazole (3 g, 29.6 mmol) and 1-bromododecane (7.4 g, 30.0 mmol). Yield = 90%. $^1$H NMR (298 K, 200 MHz, DMSO-$d_6$) $\delta$ [ppm] = 0.84 (3H, m), 1.23 (18H, m), 1.41(3H, t), 1.77 (m, 2H), 4.17 (4H, qn), 7.78 (2H, m), 9.21 (1H, s). ESI-MS (positive, ([%])) $m/z$ = 268.3 [M − Br]$^+$ (100).

*[C3C12]Br* was synthesized from 1-propylimidazole (2.5 g, 23.4 mmol) and 1-bromododecane (6.3 g, 25.7 mmol). Yield = 72%. $^1$H NMR (298 K, 200 MHz, DMSO-$d_6$) $\delta$ [ppm] = 0.83 (6H, m), 1.22 (18H, m), 1.78 (4H, m), 4.13 (4H, m), 7.81 (2H, s), 9.27 (1H, s). ESI-MS (positive, ([%])) $m/z$ = 282.3 [M − Br]$^+$ (100).

*[C4C12]Br* was synthesized from 1-butylimidazole (3 g, 24.2 mmol) and 1-bromododecane (6.6 g, 26.6 mmol). Yield = 84%. $^1$H NMR (298 K, 200 MHz, DMSO-$d_6$) $\delta$ [ppm] = 0.86 (6H, m), 1.22 (22H, m), 1.77 (4H, m), 4.17 (4H, m), 7.80 (2H, m), 9.27 (1H, s). ESI-MS (positive, ([%])) $m/z$ = 296.1 [M − Br]$^+$ (100).

*[C5C12]Br* was synthesized from 1-dodecylimidazole (3 g, 12.7 mmol) and 1-bromopentane (2.1 g, 13.9 mmol). Yield = 84%. $^1$H NMR (298 K, 200 MHz, DMSO-$d_6$) $\delta$ [ppm] = 0.84 (6H, m), 1.22 (24H, m), 1.79 (4H, m), 4.16 (4H, m), 7.82 (2H, m), 9.29 (1H, s). ESI-MS (positive, ([%])) $m/z$ = 310.3 [M − Br]$^+$ (100).

*[C6C12]Br* synthesized from 1-hexylimidazole (3 g, 19.3 mmol) and 1-bromododecane (5.0 g, 20.0 mmol). Yield = 84%. $^1$H NMR (298 K, 200 MHz, DMSO-$d_6$) $\delta$ [ppm] = 0.84 (6H, m), 1.22 (26H, m), 1.78 (4H, m), 4.16 (4H, m), 7.81 (2H, s), 9.29 (1H, s). ESI-MS (positive, ([%])) $m/z$ = 324.4 [M − Br]$^+$ (100).

*[C7C12]Br* was synthesized from 1-dodecylimidazole (3 g, 12.7 mmol) and 1-bromoheptane (2.5 g, 13.9 mmol). Yield = 84%. $^1$H NMR (298 K, 200 MHz, DMSO-$d_6$) $\delta$ [ppm] = 0.84 (6H, m), 1.22


dx.doi.org/10.1021/cg401396n | Cryst. Growth Des. 2014, 14, 1561−1571

(28H, m), 1.78 (4H, m), 4.16 (4H, m), 7.80 (2H, s), 9.25 (1H, s). ESI-MS (positive, ([%])) $m/z$ = 338.3 $[M - Br]^+$ (100).

*[C8C12]Br* synthesized from 1-octylimidazole (3 g, 16.3 mmol) and 1-bromododecane (4.1 g, 16.5 mmol). Yield = 67%. $^1$H NMR (298K, 200 MHz, DMSO-$d_6$) $\delta$ [ppm] = 0.84 (6H, m), 1.22 (30H, m), 1.78 (4H, m), 4.16 (4H, m), 7.80 (2H, s), 9.30 (1H, s). ESI-MS (positive, ([%])) $m/z$ = 352.4 $[M - Br]^+$ (100).

*[C9C12]Br* was synthesized from 1-dodecylimidazole (3 g, 12.7 mmol) and 1-bromononane (2.9 g, 13.9 mmol). Yield = 91%. $^1$H NMR (298 K, 200 MHz, DMSO-$d_6$) $\delta$ [ppm] = 0.84 (6H, m), 1.22 (32H, m), 1.78 (4H, m), 4.15 (4H, m), 7.80 (2H, s), 9.23 (1H, s). ESI-MS (positive, ([%])) $m/z$ = 366.2 $[M - Br]^+$ (100).

*[C10C12]Br* was synthesized from 1-dodecylimidazole (3 g, 12.7 mmol) and 1-bromodecane (3.1 g, 13.9 mmol). Yield = 90%. $^1$H NMR (298 K, 200 MHz, DMSO-$d_6$) $\delta$ [ppm] = 0.84 (6H, m), 1.22 (34H, m), 1.78 (4H, m), 4.12 (4H, m), 7.81 (2H, s), 9.27 (1H, s). ESI-MS (positive, ([%])) $m/z$ = 380.3 $[M - Br]^+$ (100).

*[C11C12]Br* was synthesized from 1-dodecylimidazole (3 g, 12.7 mmol) and 1-bromoundecane (3.3 g, 13.9 mmol). Yield = 90%. $^1$H NMR (298 K, 200 MHz, DMSO-$d_6$) $\delta$ [ppm] = 0.84 (6H, m), 1.22 (36H, m), 1.77 (4H, m), 4.15 (4H, m), 7.80 (2H, s), 9.23 (1H, s). ESI-MS (positive, ([%])) $m/z$ = 394.3 $[M - Br]^+$ (100).

*[C12C12]Br* was synthesized from 1-dodecylimidazole (3 g, 12.7 mmol) and 1-bromododecane (3.5 g, 13.9 mmol). Yield = 85%. $^1$H NMR (298 K, 200 MHz, DMSO-$d_6$) $\delta$ [ppm] = 0.82 (6H, m), 1.22 (38H, m), 1.77 (4H, m), 4.16 (4H, m), 7.81 (2H, s), 9.25 (1H, s). ESI-MS (positive, ([%])) $m/z$ = 408.1 $[M - Br]^+$ (100).

*[C13C12]Br* was synthesized from 1-dodecylimidazole (2 g, 9.5 mmol) and 1-bromotridecane (2.8 g, 10.5 mmol). Yield = 88%. $^1$H NMR (298 K, 200 MHz, DMSO-$d_6$) $\delta$ [ppm] = 0.85 (6H, m), 1.22 (42H, m), 1.78 (2H, m), 4.18 (4H, m), 7.80 (2H, s), 9.22 (1H, s). ESI-MS (positive, ([%])) $m/z$ = 422.4 $[M - Br]^+$ (100).

**2.3. $^1$H NMR Spectra.** were recorded on a Bruker DPX 250b (operating at 200.1 MHz for $^1$H) (Bruker, Germany).

**2.4. ESI Mass Spectra.** were recorded on an Esquire 6000 instrument (Bruker, Karlsruhe, Germany) applying the following parameters: sputtering voltage 4 kV; nebulizer pressure 10−20 psi; drying gas 5−10 L/min, 300 °C; flow rate 240 $\mu$L/h. For all mass spectrometric measurements, the ILs samples were prepared as 1 mg/mL solutions in acetonitrile.

**2.5. Crystal Structure Analysis.** Crystals of [C2C12]Br were obtained by cooling the molten compound to room temperature. Suitable single crystals were sealed in Lindeman glass capillaries. All data were collected on a Stoe IPDS-I single-crystal X-ray diffractometer with graphite monochromated Mo K$\alpha$ radiation ($\lambda$ = 0.71073 Å at 170 K). Crystal structure solution by direct methods using SIR 92 yielded the heavy atom positions. Refinement with SHELXL-97 allowed for the localization of the remaining atom positions. Hydrogen atoms were added and treated in the riding atom mode. Data reduction was carried out with the program package X-Red, and numerical absorption correction was carried out with the program X-Shape. To illustrate the crystal structures, the program Diamond 3 was used.

**2.6. Temperature-Dependent SAXS Experiments.** Small-angle X-ray scattering (SAXS) measurements were carried out at the A2 Beamline of DORIS III, Hasylab, DESY, Hamburg, Germany, at a fixed wavelength of 1.5 Å. The data were collected with a MarCCD detector. The detector was calibrated with silver behenate. The sample−detector position was fixed at 635.5 mm. For measurements, the samples were placed in a copper sample holder between aluminum foil. The sample temperature was controlled by a JUMO IMAGO 500 multichannel process and program controller. Data reduction and analysis, correction or background scattering and transmission were carried out by using the program a2tool (Hasylab).

**2.7. Differential Scanning Calorimetry (DSC).** The DSC measurements were performed with a computer-controlled Phoenix DSC 204 F1 thermal analyzer (Netzsch, Selb, D) with argon as protection gas. The samples were placed in aluminum pans which were cold-sealed under argon. Experimental data are displayed in such a way that exothermic peaks occur at negative heat flow and endothermic peaks at positive heat flow. DSC runs included heating and subsequent cooling at 5 °C/min. Given temperatures correspond to the onset of the respective thermal process.

**2.8. Polarizing Optical Microscopy.** The POM pictures of mesophases were acquired with an Axio Imager A1 microscope (Carl Zeiss MicroImaging GmbH, Göttingen, Germany) equipped with a hot stage, THMS600 (Linkam Scientific Instruments Ltd., Surrey, UK), and a Linkam TMS 94 (Linkam Scientific Instruments Ltd., Surrey, UK) temperature controller and crossed polarizers. Images were recorded at a magnification of 100× as video with a digital camera after initial heating during the cooling stage. Heating and cooling rates were 5 K/min$^{-1}$. For the measurement, the samples were placed under argon between two coverslips which were sealed with two-component adhesive (UHU plus 300, UHU GmbH & Co. KG, Bühl, Germany).

## 3. RESULTS AND DISCUSSION

**3.1. Structural Analysis.** Single crystals of compound C2C12 could be obtained from cooling the molten compound to room temperature in the form of flat, colorless needles. Experiments to obtain single crystals of the other compounds in this series of sufficient quality for X-ray structure analysis failed so far. Compound C2C12 crystallizes unexpectedly in the triclinic space group $P(\bar{1})$ (No. 2), not isotypic with C2C11,[22] which crystallizes in the monoclinic space group $P2_1/c$ (No. 14). Crystallographic data, data collection, and structure refinement details are given in Table 1. The asymmetric unit

**Table 1. Crystallographic and Refinement Details for C2C12**

| | |
|---|---|
| empirical formula | $C_{17}H_{33}BrN_2$ |
| formula weight | 345.35 g/mol |
| crystal system | triclinic |
| space group | $P\bar{1}$ |
| unit cell dimensions | $a$ = 11.0090 Å; $b$ = 12.1650 Å; $c$ = 23.1770 Å; $\alpha$ = 94.727°; $\beta$ = 95.591°; $\gamma$ = 110.903° |
| volume | 2862.9 Å |
| $Z$ | 6 |
| temperature | 170 K |
| calculated density | 1.20 mg/cm$^3$ |
| absorption coefficient | 2.149 mm$^{-1}$ |
| Θ-range for data collection | 2.3 to 25.0° |
| reflections collected/unique | 9477/6258 |
| refinement method | full-matrix least-squares on $F^2$ |
| data/parameters | 6258/547 |
| goodness-of-fit on $F^2$ | 0.785 |
| final $R$ indices [$I > 2\sigma(I)$] | $R_1$ = 0.029; $wR_2$ = 0.056 |
| $R$ indices (all data) | $R_1$ = 0.055; $wR_2$ = 0.060 |

contains three crystallographically independent $[C2C12]^+$ cations and three $Br^-$ as counterions (Figure 1). In contrast to compound C2C11, in which all undecyl chains form a linear structure of favored all-trans configurations, in C2C12 distinct differences conformations of each of the three crystallographically independent cations in the asymmetric unit are apparent.

One of the cations can be characterized by a rodlike shape with one dodecyl chain and one ethyl chain being almost perpendicular to the imidazolium core plane. Both starting C


dx.doi.org/10.1021/cg401396n | Cryst. Growth Des. 2014, 14, 1561−1571

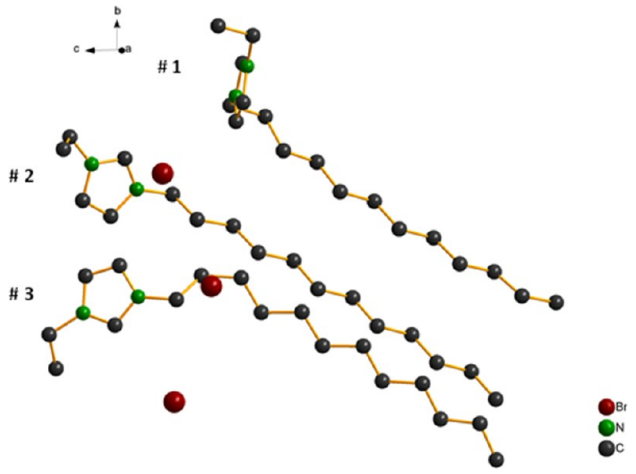


**Figure 1.** Asymmetric unit of C2C12; hydrogens are omitted for clarity.

atoms in the two alkyl chains are located in the same plane as the imidazolium core. The dodecyl chain and imidazolium core plane form an angle (defined as the angle between the imidazolium ring centroid and the terminal C atom of alkyl chain) of 95°. The terminal C atom of ethyl chain is tilted with respect to the imidazolium ring at an angle of 111°. The dodecyl chain shows all-trans conformation, aside the bond between the first and the second C atoms, which exhibits a trans−gauche conformation with a torsion angle of 62°. The imidazolium core plane is almost parallel to the *ab* plane, forming an angle of 6°.

In the second $[C2C12]^+$ cation, the angle between the dodecyl chain and imidazolium core plane increases to 143°. The terminal C atom of ethyl chain forms an angle of 110° with respect to the imidazolium. The dodecyl chain adopts an all-trans conformation. The imidazolium core plane tilts with respect to the *ab* plane at an angle of 59°.

The third $[C2C12]^+$ cation adopts a similar conformation to the second one, aside from a gauche conformation around the bond between the second and the third C atoms in the dodecyl chain, with a torsion angle of 74°. The angle between the imidazolium core plane and the *ab* plane is 76°.

The all-trans sections of the dodecyl chains belonging to the first and second cations lie in planes roughly parallel to one another and to the crystallographic *a*-axis, while that of the third cation lies roughly parallel to the crystallographic *b*-axis.

Compound C2C12 forms a layered structure, in which hydrophilic and hydrophobic regions can be observed. The hydrophobic regions are formed by interdigitated dodecyl chains of imidazolium cations with a repeating layer distance of 25.4 Å. Three cations form a unit, and units layer with different orientations (Figure 2). The interdigitation is observed in both the crystallographic *ac* and *bc* planes. The hydrophilic regions are formed by the charged imidazolium cations with the ethyl chains and bromide anions. Nonclassical hydrogen bonds between cations and anions can be discussed. Five neighboring imidazolium rings can be connected to a bromide anion via hydrogen bonds. Not only the protic C-positions on the imidazolium cores but also protons from both starting C atoms on ethyl and dodecyl chains participate the hydrogen bonding (Figure 3, top). The hydrogen bonds force the trication units to take the following conformation: the imidazolium ring in the first cation facing the imidazolium core in the third one, with a

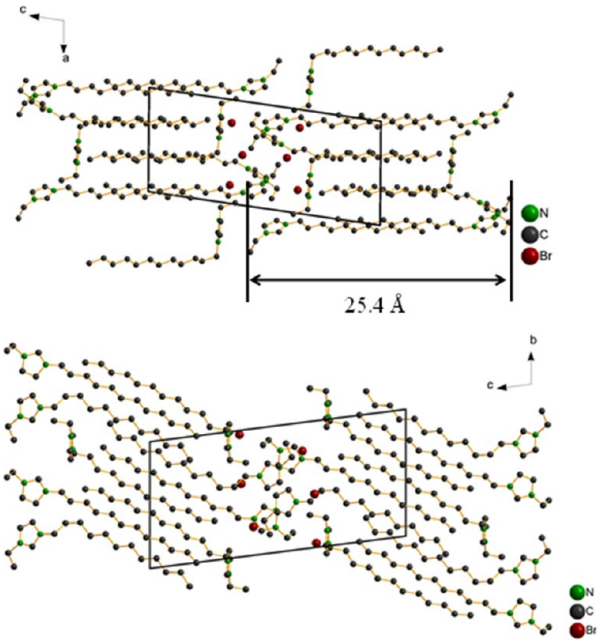


**Figure 2.** Packing diagram of C2C12. View along the crystallographic *b* axis (top) and *a* axis (bottom).

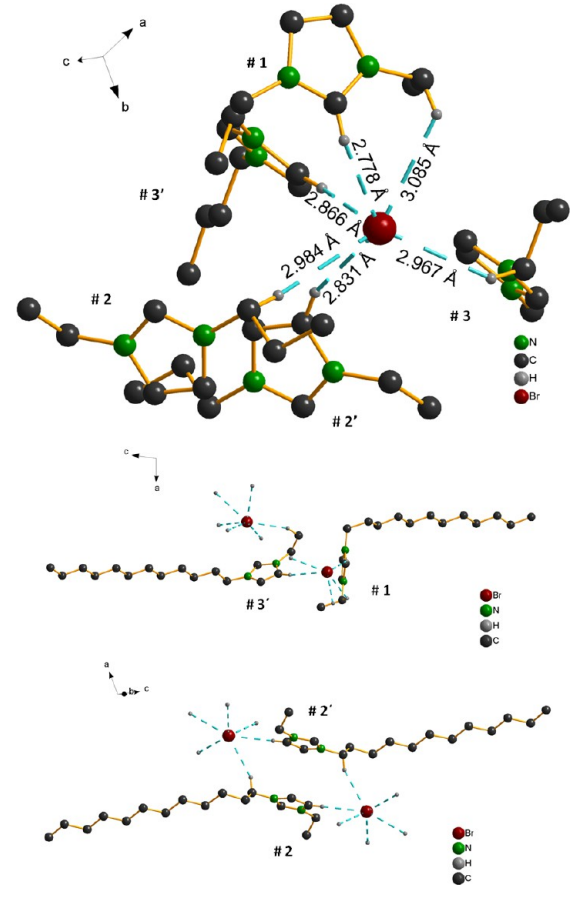


**Figure 3.** Hydrogen bonding interactions in detail for C2C12 (top); conformations of the cation units, due to hydrogen bonding (middle and bottom).

tilting angle of 70° (Figure 3, middle); the two imidazolium rings of the second cations stay parallel to each other and take a


dx.doi.org/10.1021/cg401396n | *Cryst. Growth Des.* 2014, 14, 1561−1571

face-to-face conformation (Figure 3, bottom). The hydrogen bonding interactions are summarized for clarity in Table 2.

**Table 2. Hydrogen Bonds in C2C12**

| | D−A/Å | D−H/Å | H···A/Å | D−H···A/° |
|---|---|---|---|---|
| $C_17-H_17\cdots Br$ | 3.709 | 0.970 | 3.085 | 123.379 |
| $C_12-H_12\cdots Br$ | 3.502 | 0.930 | 2.778 | 135.414 |
| $C_28-H_28B\cdots Br$ | 3.896 | 0.970 | 2.984 | 157.144 |
| $C_38-H_38B\cdots Br$ | 3.739 | 0.970 | 2.967 | 137.352 |
| $C_25'-H_25'\cdots Br$ | 3.711 | 0.930 | 2.832 | 158.231 |
| $C_35'-H_35'\cdots Br$ | 3.785 | 0.930 | 2.866 | 169.933 |

**3.2. Thermal Investigations.** The thermal properties of all compounds were investigated by polarizing optical microscopy (POM) and differential scanning calorimetry (DSC). Thermal transitions are summarized in Table S1 (see Supporting Information). The existence of mesophases was examined with POM and SAXS measurements.

For clarity, we will discuss these compounds in five separate groups according to their characteristic thermal behavior.

The first group contains compounds C0C12, C1C12, and C2C12. Their DSC scans at 5 K/min are shown in Figure 4.

All these three compounds show suppression of crystallization. In the first heating scan, the crystalline solids, as obtained from the synthesis, show a clear endothermic transition around 40 °C, which can be identified as a melting point. In contrast to C2C12, compounds C0C12 and C1C12 exhibit a liquid crystalline state. For these two compounds, small endothermic transitions are apparent at 87 °C for C0C12 and 100 °C for C1C12, which can be determined to be liquid crystalline ↔ isotropic liquid (LC ↔ L) transitions. The LC ↔ L transitions for both C0C12 and C1C12 reverse in the cooling scans with almost the same enthalpies. An extensive supercooling of the crystallization process was observed for all three compounds. However, the enthalpy value of LC ↔ S transitions, or L ↔ S transition in the case of C2C12, is significantly smaller than the value from the heating scans. In the second heating runs, a cold crystallization process preceding the melting transitions is observed for C0C12 and C2C12, and for C1C12 two of these are observed. These effects could be determined as solid−solid transitions (S ↔ S) by POM and SAXS, due to an order−disorder transition of the long alkyl chains. All further heating cycles were reproducible and similar to the first cooling and second heating scans.

The second group is comprised of compounds C3C12, C4C12, and C5C12, which are liquids at room temperature and show liquid crystalline behavior during the second heating run at lower temperature. All the following heating and cooling DSC traces are identical to the traces from the first cycle. To elucidate the thermal behavior of these compounds, POM investigations were performed. The traces from second heating and cooling scans with the corresponding POM images are shown in Figure 5. POM analyses of these samples consistently show the characteristic focal conical textures of a SmA phase. In the first cooling scans, C3C12, C4C12, and C5C12 crystallized at −39 °C, −37 °C, and −19 °C, respectively. During the second heating, they show a liquid crystalline behavior after an endothermic peak (see POM image in Figure 5). Compound C4C12 exhibits even a cool crystallization prior to this S ↔ LC transition, which could be observed from the POM measurement. While the compounds C3C12 and C4C12 are situated in liquid crystalline state, another exothermic transition is

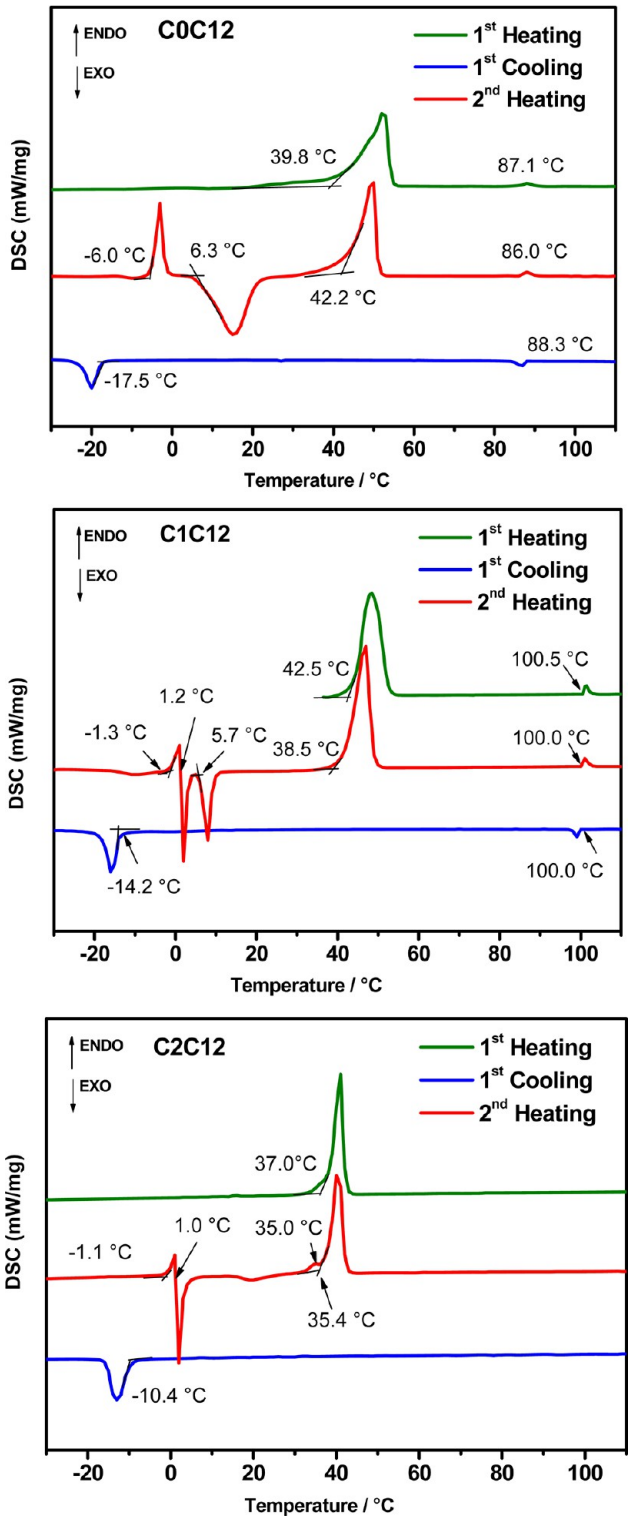


**Figure 4.** DSC scans for C0C12, C1C12, and C2C12 at 5 K/min.

observed before they melt into isotropic liquids. No visible change could be observed for this thermal effect by POM and SAXS measurements (vide infra). It could be associated to the formation of another mesophase with similar order. Since no texture changes have been observed in POM, we believe this unidentified mesophase could be considered as a smectic phase, too. For compound C5C12, a broad endothermic effect corresponding to a melting process appears at 7.5 °C with a shoulder peak at 18 °C, which can be considered as two back-


dx.doi.org/10.1021/cg401396n | Cryst. Growth Des. 2014, 14, 1561−1571

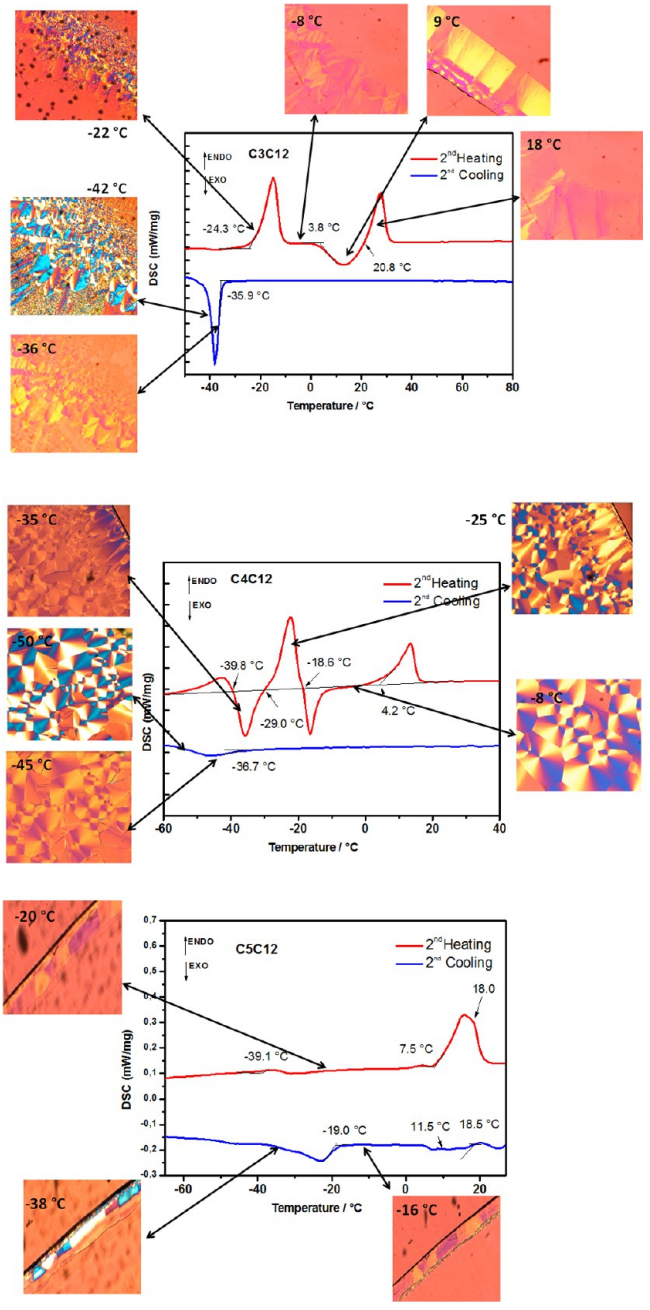


**Figure 5.** DSC thermograms of C3C12, C4C12, and C5C12 with corresponding POM images.

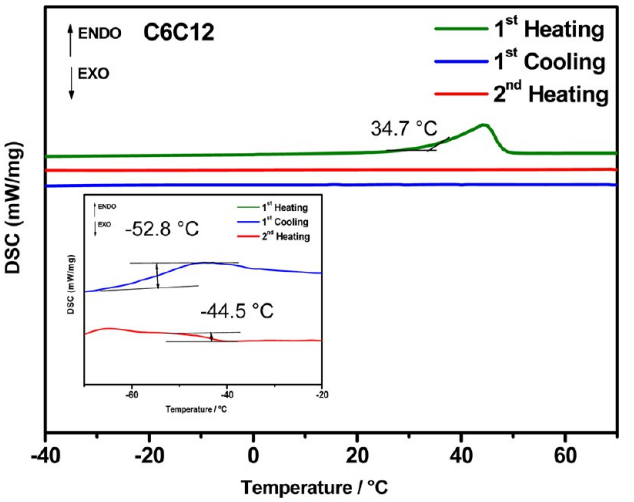


**Figure 6.** DSC scans for C6C12 at 5 K/min. Inset shows an enlarged view of DSC scans in the region of the glass transitions.

to-back thermal effects. These two transitions are observed separately in the cooling scans, as a result of supercooling. This transition can be considered as the transition between the unidentified mesophases, SmX ↔ SmA.

Surprisingly, compound C6C12 does not show any liquid crystalline properties. The thermal behavior corresponds to a typical IL. Crystals of C6C12 were obtained by recrystallization from solution. During the first heating DSC scan, a clear melting point is shown at 35 °C. Once molten, the DSC shows only a glass transition in the thermal cycle. Obviously, the recrystallization from the melt is hindered. The thermal behavior of C6C12 illustrated in Figure 6.

The fourth group contains compounds C7C12, C8C12, C9C12, and C10C12. Generally, the DSC traces are simple and show two transitions, the melting point (S ↔ LC transition) and the clearing point (LC ↔ L-transition). C7C12 and C8C12 show only a broad endothermic peak in the first heating scans, which is a result of two overlapping thermal effects. These two effects are observed separately in the cooling scans, due to supercooling. For C8C12, these two effects are visible as two successive narrow peaks in the second heating scan. Further heating and cooling cycles of C8C12 show thermal behavior identical to the first cooling and second heating scans. For C7C12, C9C12, and C10C12, all the subsequent thermal cycles are identical to the first heating cycle. The traces from the second heating cycle are shown in Figure 7.

C11C12, C12C12, and C13C12 make up the final group. All of these compounds show only melting points (S ↔ LC transition) and clearing points (LC ↔ L-transition) in the first heating scans. In the cooling scan, they display crystal polymorphism. At lower temperature, multiple transitions are visible in the DSC traces, which can be attributed to crystal−crystal transitions. These thermal effects are reversed in the second heating run. For C12C12 and C13C12, exothermic S ↔ S transitions preceding the melting points are observed (Figure 8).

The temperature range (obtained from the collected thermal data of the melting points (S ↔ LC or S ↔ L-transition) and clearing points (LC ↔ L-transition)) of mesophase for all the compounds is shown in Figure 9. Two significant trends for both melting point and clearing point are observed on either side of $n = 6$: for $1 \leq n \leq 5$ the transition temperatures decrease with increasing chain length; after $n < 6$, the inverse trend is observed. This effect is in agreement with the observations of Rocha et al. for 1-alkyl-3-methylimidazolium bis-(trifluoromethanesulfonyl)imide salts.[24] Inverse trends both in enthalpies and entropies with the increase of the cation alkyl chain length either side of 1-hexyl-3-methylimidazolium cation have been reported. The trend changes around $n = 6$ can be related to structural modifications and indicate the beginning of a new regular type of molecular interaction. The falling trends up to $n = 6$ can be explained by considering the decreasing van der Waals forces between the long alkyl chains, as shorter alkyl chains are brought into and disrupt the highly ordered dodecyl chain stacks. The discontinuity observed at $n = 6$ could be due to compensation of destructive interactions from disorder of shorter alkyl chains by cohesive forces from ordered dodecyl


dx.doi.org/10.1021/cg401396n | Cryst. Growth Des. 2014, 14, 1561−1571

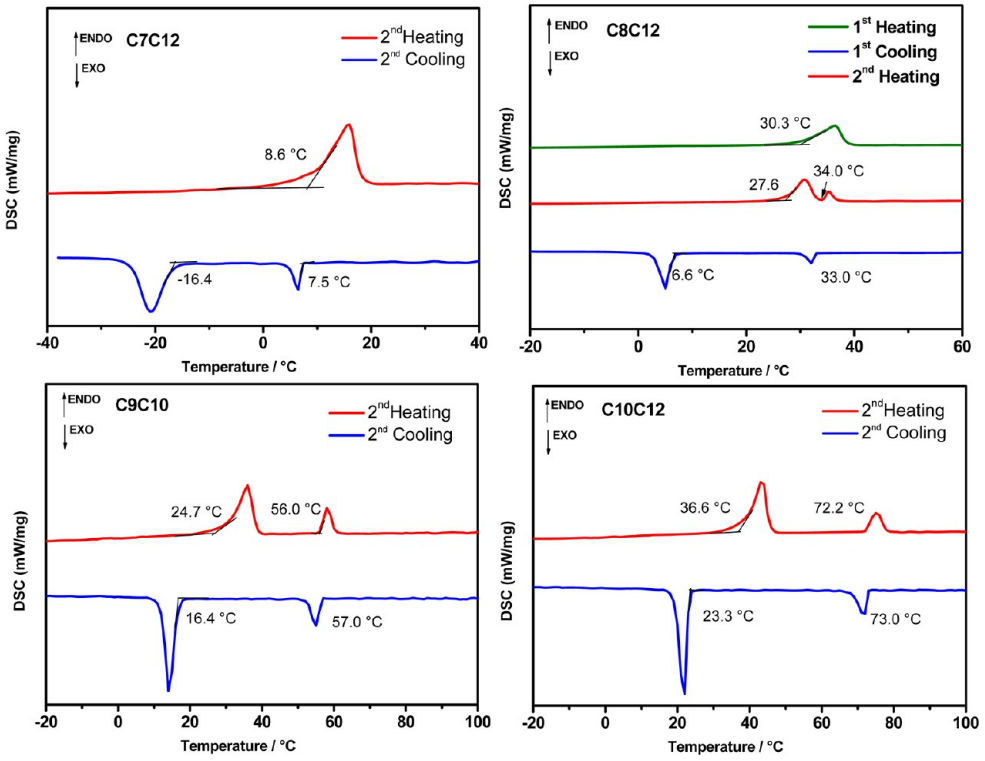


**Figure 7.** DSC scans for C7C12, C8C12, C9C12, and C10C12 at 5 K/min.

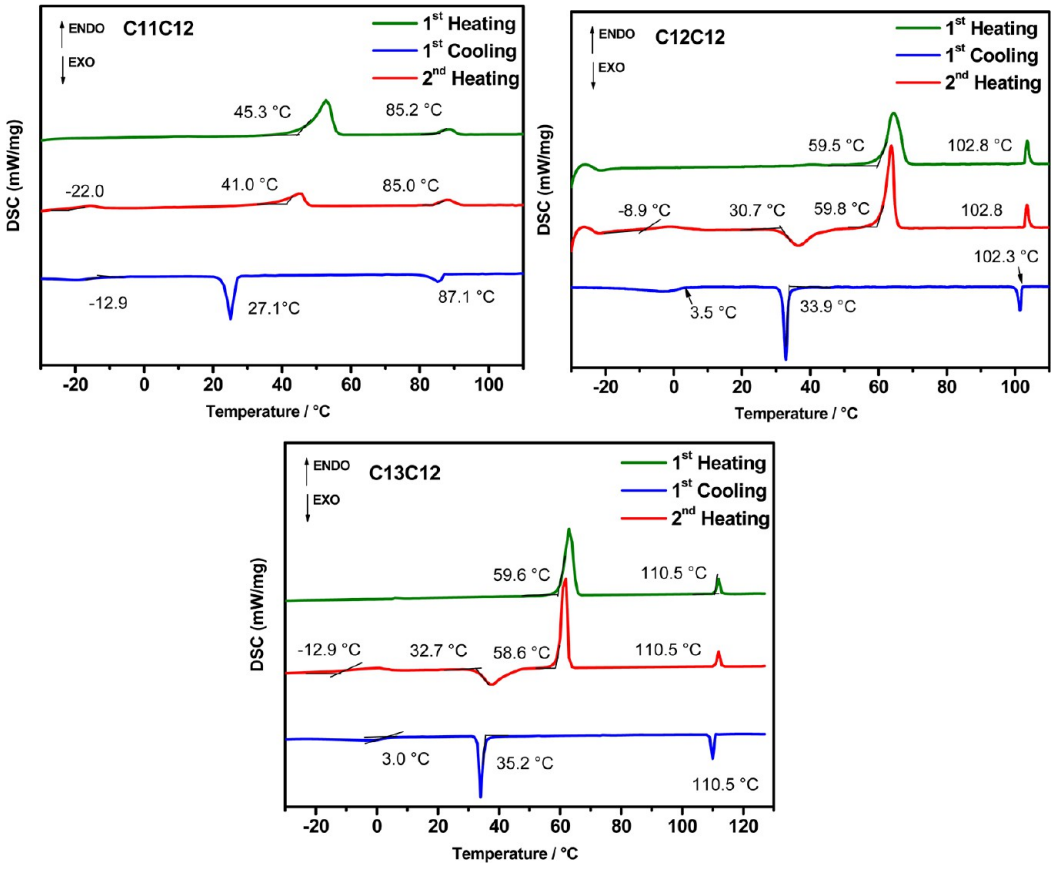


**Figure 8.** DSC scans for C11C12, C12C12, and C13C12 at 5 K/min.

chains. For $n > 6$, the cohesive intermolecular interactions through van der Waals forces rise with each additional $-CH_2-$ group. Remarkably, C6C12 exhibits a similar melting point to those of C0C12, C1C12, and C2C12. This indicates the hexyl


dx.doi.org/10.1021/cg401396n | *Cryst. Growth Des.* 2014, 14, 1561−1571

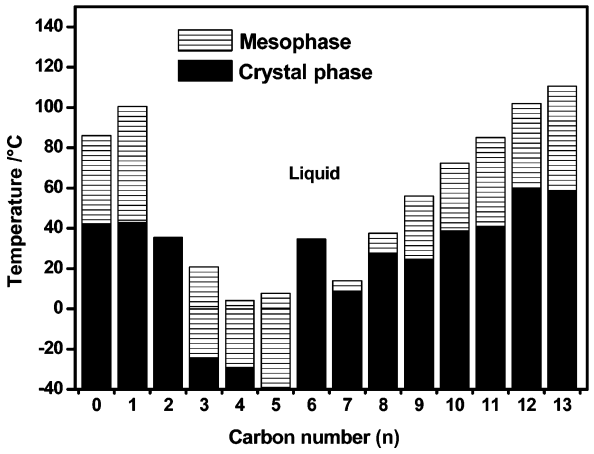


**Figure 9.** The phase transition diagram of [CnC12]Br from DSC at 5 °C/min. For compound C6C12, the value from first DSC heating scan was taken. For the rest of the compounds, all the transitions are reversible, and the thermal data from the second heating scans were taken. For clarity, the solid−solid and LC−LC transitions are not shown.

groups could be packed into a crystal lattice almost as well as methyl or ethyl groups, offering an explanation for the discontinuity at this value. The same effect of hexyl groups has been observed by Dzyuba et al. for symmetrical 1,3-dialkylimidazolium hexafluorophosphate.[25] A well-packed crystal lattice probably exhibiting low flexibility, could explain why C6C12 is not favored for mesophase formation. In addition, we observed a distinct odd−even effect for $5 \leq n \leq 10$ in the melting transitions, which is reflected in the state of the compounds at room temperature. The melting points of the compounds with even $n$ are higher than their immediate neighbors with odd lengths of $n$. C5C12, C7C12, and C9C12 exist as viscous but fluid liquids, while C6C12, C8C12, and C10C12 are wax-like solids (Figure 10). This phenomenon is

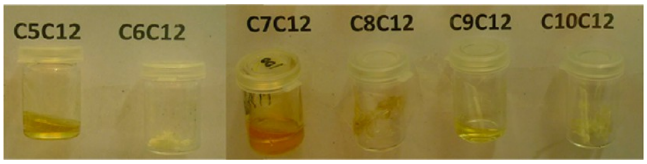


**Figure 10.** Demonstration of even−odd-effect: compounds C5C12, C6C12, C7C12, C8C12, C9C12, and C10C12 at room temperature.

contrary to the even−odd effect discussed by Holbrey and Seddon for 1-alkyl-3-methylimidazolium with long chains.[6] Our observation could be a reflection of the ion dynamics in ILs, which has also been observed for viscosity with a similar even−odd effect.[26] A high local order in systems with even chain lengths observed by MD simulations was reported by Wang and Voth; they showed the diffusion constants of compounds with odd alkyl chain lengths are smaller than the diffusion constants of compounds with even chain lengths.[27] In contrast, the clearing points increase rapidly with rising $n$, for $n \geq 7$, and no even−odd effect is observed.

**3.3. Mesophase Investigations with POM and SAXS.** Liquid crystalline mesophases were observed during the process of heating and cooling for all compounds except C2C12 and C6C12. The temperature ranges and the existence of the aforementioned mesophases for the 12 compounds were confirmed by polarizing optical micrographs and X-ray scattering in the small angle range. The corresponding POM images for all the mesogens are shown in Figure 11. Compounds C0C12, C5C12, C8C12, and C12C12 show an oily streak texture, and the other compounds show a focal conic fan texture. Both textures indicate a smectic mesophase. The layer spacing distances $d$ of all the compounds in the crystalline states and the ionic liquid crystalline phases are summarized in Table 3.

The SAXS data supply an insight into the alignment in crystalline and liquid crystalline states. For clarity, the layer spacing distances $d$ of all the compounds in the crystalline states and the ionic liquid crystalline phases are plotted with $n$, the length of the varying alkyl chain is shown in Figure 12. As is well-known, imidazolium-based ILs with long alkyl chains form layered structures by interdigitating the long alkyl tails. During heating and cooling processes, the rod-shaped molecules move along the alkyl axis, so that the attractive van der Waals forces maintain a mesophase formation.[28] The layer spacing increases on transforming from the crystal to the mesophase for compound C0C12, C1C12, C12C12, and C13C12, which indicates that the structure undergoes a formation of smectic A phase by decreasing the angle of tilt with respect to the layer normal and/or decreasing of the interdigitated region. For compounds C7C12, C8C12, C9C12, C10C12, and C11C12, the layer spacing in the mesophase is smaller than the layer spacing in the crystal. This indicates that in the mesophase, the alkyl chains of cations are tilted with respect to the layer normal. In this way, a smectic C phase is formed. Smaller $d$ values in the crystalline state indicate a high extent of alkyl chain interdigitation, which creates greater cohesive intermolecular interactions. These strong interactions lead to a higher melting point. The $d$ values in crystalline phases for compounds C3C12, C4C12, and C5C12 could not be measured, since their crystallizations occur at very low temperatures, which were not accessible under the given experimental conditions. The structural relationship between the crystalline and liquid crystalline states can be discussed for $n \leq 2$ and $6 \leq n \leq 13$. The layer spacing increases by ca. 4 Å from C0C12 to C1C12. It could be argued as a consequence of the reorganization due to the addition of a methyl group. The layer distance increases from $n = 1$ to $n = 2$ by around 1.5 Å, corresponding roughly to the length of a $-CH_2-$ group. The lowest $d$ value is observed for $n = 6$. This confirms the previous declaration: Hexyl groups pack well into the crystal lattice. Full interdigitation is necessary to counteract the destructive interactions. From $n = 7$ to $n = 9$, the value of $d$ rises again by 1.5 Å with the addition of each methylene unit. The lower value at $n = 10$ compared to its immediate neighbors with odd alkyl chain lengths is indicative of significant interdigitation of alkyl chains and thus fortified van der Waals forces. This is in agreement with our observation of a higher melting point. The dramatic fall of around 8.5 Å from $n = 11$ to $n = 12$ and the sharp rise of 5 Å from $n = 12$ to $n = 13$ could possibly be associated with a twist of the alkyl chains, meaning that the molecules adopt a V-shape instead of linear rod shape. Formation of a V-shape for compound [C12C12]I has been reported by Wang et. al.[29] Since the layer spacing of C0C12 and C12C12 is quite similar, we believe their alkyl chains must be tilted with respect to the layer normal at the same angle. The conformations of these two compounds are illustrated in Figure 13.

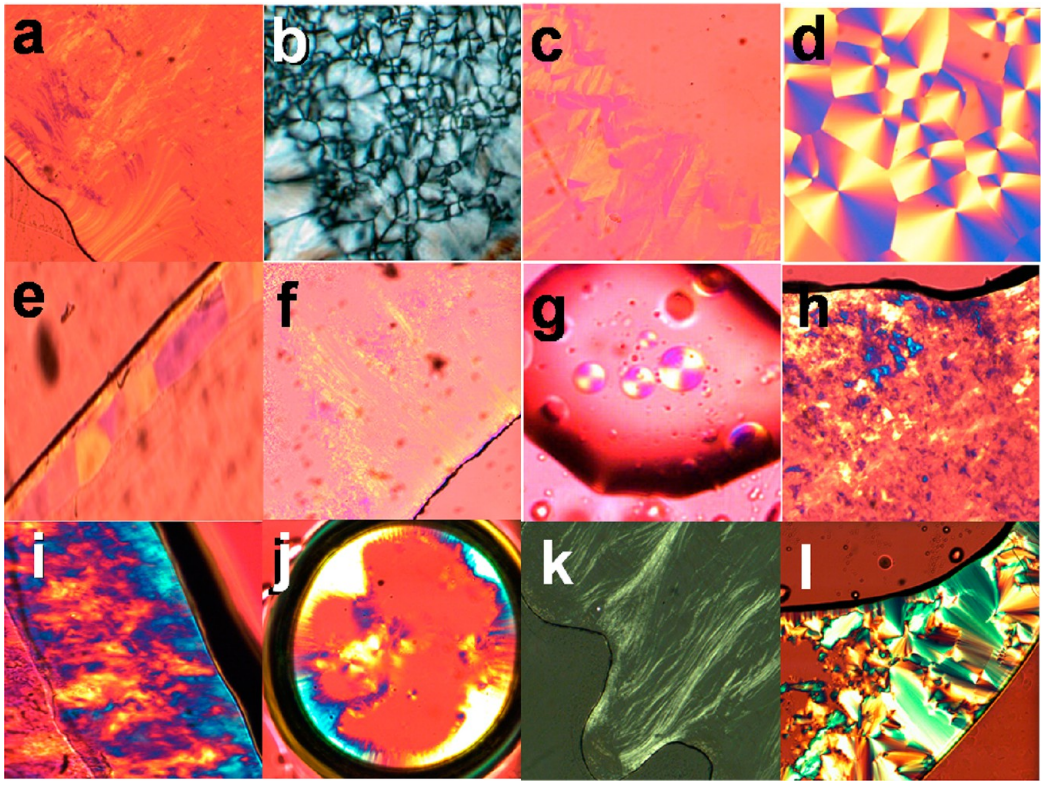


**Figure 11.** Polarizing optical microscopy images: (a) C0C12 at 56 °C; (b) C1C12 at 67 °C; (c) C3C12 at −8 °C; (d) C4C12 at −10 °C; (e) C5C12 at −20 °C; (f) C7C12 at 0 °C; (g) C8C12 at 25 °C; (h) C9C12 at 40 °C; (i) C10C12 at 60 °C; (j) C11C12 at 70 °C; (k) C12C12 at 60 °C; (l) C13C12 at 40 °C.

**Table 3. Layer Distances *d*/Å in the Crystalline States and the Liquid Crystalline Phases**

| | C0C1 | C1C12 | C2C12 | C3C12 | C4C12 | C5C12 | C6C12 |
|---|---|---|---|---|---|---|---|
| $d_{Cr}$ [Å] | 20.6 | 24.4 | 26.2 | b | b | b | 16.5 |
| $d_{LC}$ [Å] | 29.9 | 29.5 | a | 29.6 | 24.8 | 25.0 | a |
| | C7C12 | C8C12 | C9C12 | C10C12 | C11C12 | C12C12 | C13C12 |
| $d_{Cr}$ [Å] | 25.4 | 26.8 | 28.3 | 25.8 | 27.4 | 19.1 | 24.2 |
| $d_{LC}$ [Å] | 23.3 | 23.4 | 23.3 | 23.9 | 25.5 | 28.0 | 33.4 |

## 4. CONCLUSIONS

We have attempted to determine the essential parameters for mesophase formation of imidazolium-based ILs by varying the cation geometry. According to the results from previous report,[22] N-dodecyl chains appear to be essential for mesomorphic behavior. Therefore, a library of 14 1-alkyl-3-dodecylimidazolium based bromides salts was synthesized. The thermal transitions and liquid crystalline behavior have been studied by DSC, POM, and SAXS. The structure of compound C2C12 could be obtained from the single crystal X-ray analysis.

Compound C2C12 crystallizes in the triclinic space group $P(\bar{1})$ (No. 2). The asymmetric unit contains three cations with distinct conformations in contrast to compound C2C11,[22] in which all undecyl chains form a linear moiety of favored all-trans configurations.

All the compounds can be considered as ILs, as their melting points are below 100 °C. Thermotropic liquid crystalline behavior can be observed for all the compounds except C2C12 and C6C12. On the basis of their distinct thermal behavior, these salts can be described in four groups: (i) materials with surpressed crystallization; (ii) compounds that are liquid at room temperature and exhibit cold crystallization during the second heating run at lower temperature (≤−20 °C); (iii) C6C12, an IL exhibiting a melting point in the first heating scan and only glass transitions in following heating cycles; (iv) compounds displaying crystalline polymorphism at lower temperature.

The variation of the melting points with chain length *n*, where *n* is the length of the varying alkyl chain, shows clearly two trends: For $1 \leq n \leq 5$, the melting point decreases with increasing *n*. This can be explained by considering the decreasing van der Waals forces between the long alkyl chains, as shorter alkyl chains are brought into and disrupt the highly ordered dodecyl chain stacks.

The trend changes around $n = 6$ can be related to structural modifications and indicate the beginning of a new regular type of molecular interaction. For $n > 6$, the melting points increases with increasing *n*, due to the increasing van der Waals forces between the long alkyl chains by addition of $-CH_2-$ group. Furthermore, we observed an odd−even effect for $5 \leq n \leq 10$ in the melting transitions. The fact that the melting points of the compounds with even *n* are higher than their immediate neighbors with odd lengths of *n* is surprising at first glance but can be rationalized in terms of ion dynamics and in light of MD simulations.[26,27]


dx.doi.org/10.1021/cg401396n | *Cryst. Growth Des.* 2014, 14, 1561−1571

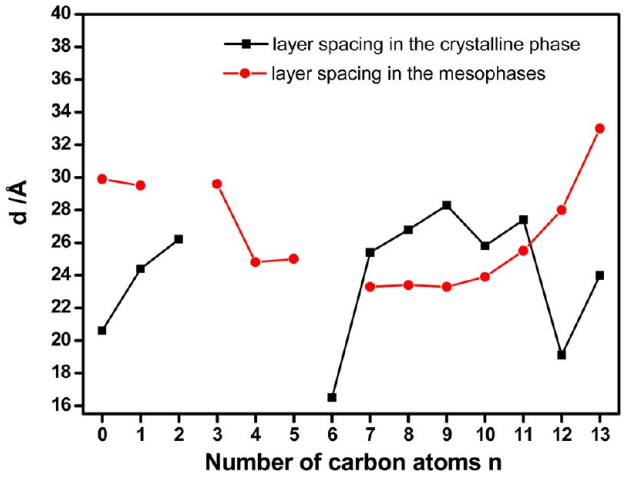


**Figure 12.** Schematic representation of the layer spacing distances *d* [Å] of all the compounds in the crystalline and the ionic liquid crystalline states. The layer spacing in crystalline states is plotted in black and in liquid crystalline phases in red. Only the *d* values obtained from the (001) reflections are shown. For compounds C2C12 and C6C12, no mesophase was observed. For compound C3C12 and C4C12, and C5C12, no layer spacing could be measured due to the experimental limits and low crystallization temperatures. For compounds exhibiting more than one crystalline polymorph at low temperatures, only the *d* spacing at room temperature was given.

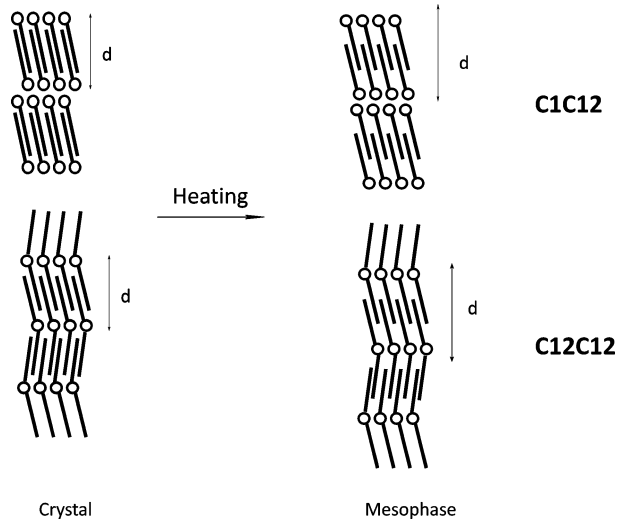


**Figure 13.** Illustration of the changes in the molecular arrangement of C0C12 and C12C12 from the crystalline state to the mesophase.

The liquid crystalline properties of mesomorphic compounds were examined by differential scanning calorimetry and polarized optical microscopy. Combing the informations obtained from POM images and X-ray scattering experiments at small angle range, the mesophases that they form can be identified as the smectic phase for these compounds. Observations from SAXS measurements indicate that C0C12, C1C12, C12C12, and C13C12 form smectic A phase, while C7C12, C8C12, C9C12, C10C12, and C11C12 show smectic C formations. Unequivocal mesophase identification for compounds C3C12, C4C12, and C5C12 is not possible due to the low temperature transitions lying beyond experimental limits.

Finally, no thermic mesophase formation was observed for C2C12 and C6C12. However, both of the compounds contain dodecyl units, which should according to our conclusions from section 2 arouse a mesophase. This indicates the inadequacy of a dodecyl group in guaranteeing mesophase formation. Crystal structure analysis shows for C2C12 a bilayer lamellar structure with a separation of hydrophobic (alkyl chains stacks) and hydrophilic (imidazolium head groups) regions in the cations. Remarkably, the arrangement of imidazolium cores in the hydrophilic parts is very complicated, due to multiple nonclassical hydrogen bonds between bromide anions and imidazolium head groups, which hinder intensive interdigitations of long chains. Therefore, we propose that a similar system with less hydrogen bonds in the hydrophilic region could improve liquid crystalline properties. Our further work will focus on reducing the number of H-bond donors in the hydrophilic core by replacing the 2-H proton on the imidazolium cation by a methyl group. Additional experiments on similar 2-methylimidazolium-based ILs bearing a dodecyl group with different sizes and symmetries are required to gauge the importance of such H-bond interactions.

## ■ ASSOCIATED CONTENT

### Supporting Information

Table S1: Thermal behavior of *n*-alkyl-dodecylimidazolium bromide ionic liquids and ionic liquid crystals; SAXS measurements; synthesis of 1-dodecylimidazole; crystallographic information file. This material is available free of charge via the Internet at http://pubs.acs.org.

## ■ AUTHOR INFORMATION

### Corresponding Author

*E-mail: anja.mudring@ruhr-uni-bochum.de. Tel: +49-234-32-27408.

### Notes

The authors declare no competing financial interest.

## ■ ACKNOWLEDGMENTS

This work was supported by the German Science Foundation DFG through the priority program 1191"Ionic Liquids", the DFG Cluster of Excellence RESOLV, and the DESY (Deutsches Elektronensynchrotron Proposal No. I-20100011). We thank Dr. Sergio Funari for support during the SAXS measurements and thank Dr. P. Campbell for helpful comments.

## ■ REFERENCES

(1) Binnemans, K. *Chem. Rev.* **2005**, *105*, 4148−4204.
(2) Holbrey, J. D.; Rogers, R. D. In *Ionic Liquid in Synthesis*; Wasserscheid, P., Welton, T., Eds.; Wiley-VCH, Weinheim, 2008; Vol. *1*, pp 57−88.
(3) Tokuda, H.; Hayamizu, K.; Ishii, K.; Susan, M. A. B. H.; Watanabe, M. *J. Phys. Chem. B* **2005**, *109*, 6103−6110.
(4) Tokuda, H.; Hayamizu, K.; Ishii, K.; Susan, M. A. B. H.; Watanabe, M. *J. Phys. Chem. B* **2004**, *108*, 16593−16600.
(5) Welton, T. *Chem. Rev.* **1999**, *99*, 2071−2083.
(6) Holbrey, J. D.; Seddon, K. R. *J. Chem. Soc., Dalton Trans.* **1999**, 2133−2140.
(7) Wasserscheid, P.; Keim, W. *Angew. Chem., Int. Ed.* **2000**, *39*, 3772−3789.
(8) Yamanaka, N.; Kawano, R.; Kubo, W.; Masaki, N.; Kitamura, T.; Wada, Y.; Watanabe, M.; Yanagida, S. *J. Phys. Chem. B* **2007**, *111*, 4763−4769.
(9) Axenov, K. V.; Laschat, S. *Materials* **2011**, *4*, 206−259.
(10) Taubert, A. *Angew. Chem., Int. Ed.* **2004**, *43*, 5380−5382.

(11) Yang, M.; Campbell, P. S.; Santini, C. C.; Mudring, A. V. *Nanoscale* **2014**, DOI: 10.1039/c3nr05048c.
(12) Taubert, A.; Palivan, C.; Casse, O.; Gozzo, F.; Schmitt, B. *J. Phys. Chem. C* **2007**, *111*, 4077−4082.
(13) Douce, L.; Suisse, J.-M.; Guillon, D.; Taubert, A. *Liq. Cryst.* **2011**, *38*, 1653−1661.
(14) Yang, M.; Stappert, K.; Mudring, A.-V. *J. Mater. Chem. C* **2014**, *2*, 458−473.
(15) Lee, C. K.; Huang, H. W.; Lin, I. J. B. *Chem. Commun. (Cambridge)* **2000**, 1911−1912.
(16) Wang, X.; Sobota, M.; Kohler, F. T. U.; Morain, B.; Melcher, B. U.; Laurin, M.; Wasserscheid, P.; Libuda, J.; Meyer, K. *J. Mater. Chem.* **2012**, *22*, 1893−1898.
(17) Kohler, F. T. U.; Morain, B.; Weiss, A.; Laurin, M.; Libuda, J.; Wagner, V.; Melcher, B. U.; Wang, X.; Meyer, K.; Wasserscheid, P. *ChemPhysChem* **2011**, *12*, 3539−3546.
(18) Wang, X.; Heinemann, F. W.; Yang, M.; Melcher, B. U.; Fekete, M.; Mudring, A.-V.; Wasserscheid, P.; Meyer, K. *Chem. Commun.* **2009**, 7405−7407.
(19) Fox, D. M.; Awad, W. H.; Gilman, J. W.; Maupin, P. H.; De, L. H. C.; Trulove, P. C. *Green Chem.* **2003**, *5*, 724−727.
(20) De, R. J.; Gordon, C. M.; Imrie, C. T.; Ingram, M. D.; Kennedy, A. R.; Lo, C. F.; Triolo, A. *Chem. Mater.* **2003**, *15*, 3089−3097.
(21) Lee, K.-M.; Lee, Y.-T.; Lin, I. J. B. *J. Mater. Chem.* **2003**, *13*, 1079−1084.
(22) Yang, M.; Mallick, B.; Mudring, A.-V. *Cryst. Growth Des.* **2013**, *13*, 3068−3077.
(23) Yamanaka, N.; Kawano, R.; Kubo, W.; Kitamura, T.; Wada, Y.; Watanabe, M.; Yanagida, S. *Chem. Commun.* **2005**, 740−742.
(24) Rocha, M. A. A.; Lima, C. F. R. A. C.; Gomes, L. R.; Schröder, B.; Coutinho, J. A. P.; Marrucho, I. M.; Esperança, J. M. S. S.; Rebelo, L. P. N.; Shimizu, K.; Canongia Lopes, J. N.; Santos, L. M. N. B. F. *J.Phys. Chem. B* **2011**, *115*, 10919.
(25) Dzyuba, S. V.; Bartsch, R. A. *Chem. Commun.* **2001**, 1466−1467.
(26) Zheng, W.; Mohammed, A.; Hines, L. G.; Xiao, D.; Martinez, O. J.; Bartsch, R. A.; Simon, S. L.; Russina, O.; Triolo, A.; Quitevis, E. L. *J. Phys. Chem. B* **2011**, *115*, 6572−6584.
(27) Wang, Y.; Voth, G. A. *J. Phys. Chem. B* **2006**, *110*, 18601−18608.
(28) Bradley, A. E.; Hardacre, C.; Holbrey, J. D.; Johnston, S.; McMath, S. E. J.; Nieuwenhuyzen, M. *Chem. Mater.* **2002**, *14*, 629−635.
(29) Wang, X.; Vogel, C. S.; Heinemann, F. W.; Wasserscheid, P.; Meyer, K. *Cryst. Growth Des.* **2011**, *11*, 1974.